CHRONOBIOLOGY INTERNATIONAL
https://doi.org/10.1080/07420528.2021.1903027

Taylor & Francis
Taylor & Francis Group

Circadian clock modulating small molecules repurposing as inhibitors of SARS-CoV-2 M^{pro} for pharmacological interventions in COVID-19 pandemic

Armiya Sultan[a,b,c], Rafat Ali[b], Tahira Sultan[d], Sher Ali[e], Nida Jamil Khan[b], and Arti Parganiha[c]

[a]Functional Genomics Laboratory, Center for Interdisciplinary Research in Basic Sciences, Jamia Millia Islamia (A Central University), New Delhi, India; [b]Department of Biosciences, Jamia Millia Islamia (A Central University), New Delhi, India; [c]Chronobiology and Animal Behaviour Laboratory, School of Studies in Life Sciences, Pt. Ravishankar Shukla University, Raipur, India; [d]Department of Biochemistry, University of Kashmir, Srinagar, India; [e]Department of Life Sciences, Sharda University, Greater Noida, India

ABSTRACT

The COVID-19 pandemic caused by SARS-CoV-2 is a global health emergency warranting the development of targeted treatment. The main protease M^{pro} is considered as a key drug target in coronavirus infections because of its vital role in the proteolytic processing of two essential polyproteins required for the replication and transcription of viral RNA. Targeting and inhibiting the M^{pro} activity represents a valid approach to prevent the SARS-CoV-2 replication and spread. Based on the structure-assisted drug designing, here we report a circadian clock-modulating small molecule "SRT2183" as a potent inhibitor of M^{pro} to block the replication of SARS-CoV-2. The findings are expected to pave the way for the development of therapeutics for COVID-19.

ARTICLE HISTORY
Received 13 July 2020
Revised 5 March 2021
Accepted 9 March 2021

KEYWORDS
Circadian clock-modulating molecules; COVID-19; inhibitors; main protease; pandemic; SARS-CoV-2 M^{pro}; SRT2183; targeted therapy

Introduction

Outbreaks of deadly contagious diseases, particularly caused by viruses, have always been a big threat to the human race. During the last five decades, herpes, legionnaires, HIV/AIDS, Western African Ebola epidemic, Middle East Respiratory Syndrome (MERS), Severe Acute Respiratory Syndrome (SARS), and now new coronavirus disease 2019 (COVID-19) viruses have attacked human population worldwide. The members of the coronavirus family, alone, have caused two deadly outbreaks, namely MERS caused by MERS coronavirus (MERS-CoV) and SARS caused by SARS coronavirus (SARS-CoV) during the last two decades (Zhong et al. 2020). In December 2019, a new unprecedented viral infection emerged in Wuhan, China. Genomic studies have shown that about 82% genome of this novel virus match the RNA genome of SARS-CoV (Wu et al. 2020a, 2020b; Zhou et al. 2020). The novel virus was named as Severe Acute Respiratory Syndrome coronavirus-2 (SARS-CoV-2) and the contagious infectious disease caused by this new virus was named as coronavirus disease 2019 (COVID-19) (Gorbalenya et al. 2020).

Pathophysiological findings made it evident that SARS-CoV-2 infection is more contagious than both MERS and SARS (Zhang and Holmes 2020). Infection can spread even if an individual is asymptomatic or in presymptomatic conditions. Individuals infected with SARS-CoV-2 develop mild-to-moderate illness; however, older people and those with chronic medical complications are more likely to develop serious illness (Chen et al. 2020; Li et al. 2020; World Health Organization, clinical management of COVID-19: Interim Guidance 2020).

In December 2019, the COVID-19 pandemic outbreak originated in Wuhan city, Hubei province of China. The first cluster of cases of "pneumonia of unknown cause" was reported in late December 2019 (Wu et al. 2020c). Thereafter, the contagious SARS-CoV-2 infection quickly spread globally. The first laboratory-confirmed novel coronavirus case recorded outside of China was reported on 13th January 2020 by the Ministry of Public Health in Thailand (Yan et al. 2020). The World Health Organization (WHO) declared the infection a pandemic on 11th March 2020 (Zhang et al. 2020). According to WHO reports, confirmed cases of COVID-19 are increasing exponentially worldwide. Globally, as of 04:02h CET, 4 March 2021, there have been 114,853,685 confirmed cases of COVID-19, including 2,554,694 deaths, reported to WHO (https://covid19.who.int/). However, these numbers are likely to be higher than reported because of the frequent exclusion of mild or asymptomatic cases.

Currently, no therapeutic options are available for COVID-19. However, an insight gained on the SARS-CoV-2 RNA genome and crystal structures of

CONTACT Armiya Sultan armia86bms@gmail.com Functional Genomics Laboratory, Center for Interdisciplinary Research in Basic Sciences, Jamia Millia Islamia (A Central University), New Delhi110025, India.

encoded translated products is envisioned to pave the way to accomplish this goal (Jin et al. 2020a; Jin, Zhou et al. 2020b; Jo et al. 2020; Zhang et al. 2020). The RNA genome of SARS-CoV-2 contains approximately 30,000 nucleotides encoding structural and non-structural proteins needed to form a functionally complete viral particle (Jin et al. 2020a; Jin, Zhou et al. 2020; Wu et al. 2020a). More importantly, the SARS-CoV-2 RNA genome encodes two polyproteins (pp) termed as pp1a (~450 kDa) and pp1ab (~750 kDa), which undergo proteolytic cleavage by main protease (M^{pro}; also known as 3 C-like protease) and a papain-like protease to form functional polypeptides required for viral replication (Hegyi and Ziebuhr 2002; Wu et al. 2020a). The M^{pro} predominantly cleaves the polyprotein at 11 conserved sites, starting with the autolytic digestion of this enzyme itself, from pp1a and pp1ab (Hegyi and Ziebuhr 2002; Jin et al. 2020a; Jin, Zhou et al. 2020). The crucial functional properties of M^{pro} make it a constructive target for the coronavirus drug discovery and development.

The study of the "clock-infection biology" of viral diseases is a relatively new emerging field. This field is intended to decipher the complex relationships between the circadian timing system, host immunity, host–virus interactions, and development of therapeutic agents (Mazzoccoli et al. 2020; Ray and Reddy 2020). This emerging field holds great potential for unraveling the complex pathogenesis of SARS-CoV-2 infection and may help to contribute better therapeutic agents against this novel pathogen (Ray and Reddy 2020). Currently, key proteins of this novel coronavirus are extensively targeted for the repurposing of the existing small molecules and other drugs as therapeutic agents for COVID-19 (Jin et al. 2020a; Jin, Zhou et al., 2020; Jo et al. 2020; Zhang et al. 2020). M^{pro} has been proposed as a central therapeutic target (Jin, Zhou et al. 2020; Pillaiyar 2016; Sisay 2020; Yang et al. 2003). In the present study, we employed the structure-assisted drug designing protocols to explore the pharmacological attributes of the existing circadian clock-modulating small molecules against SARS-CoV-2 M^{pro} for the development of therapeutics for COVID-19. The rationale of this focus is that these small molecules have shown significant inhibition or activation of proteins and enzymes of the molecular circadian clock in different clock-related chronic disease models (for supporting references, refer Table 1). In addition, many of these small molecules have been highlighted as therapeutic molecules in diseases or disorders not related to the circadian timing system (Chowdhury et al. 2020; Kim et al. 2018; Lahusen and Deng 2015; Palliyaguru et al. 2020; Scuto et al. 2013; Ye et al. 2019). Among the 24 small molecules, we found SRT2183 (binding affinity −9.2 kcal/mol) to be a potent inhibitor of M^{pro} that may be implemented to block replication of SARS-CoV-2. Findings are expected to pave the way for the development of therapeutics for COVID-19.

Materials and methods

Receptor structure preparation

The newly formulated crystal structure of the target protein SARS-CoV-2 M^{pro} in a complex with carmofur (PDB ID: 7BUY) retrieved from the RCSB PDB database was taken as a template for molecular docking studies. This protein-inhibitor complex provided a structure-assisted drug designing model for recognition of effective inhibitors of the main protease M^{pro} of SARS-CoV-2 (Jin et al. 2020b). A standard receptor preparation protocol was followed for crystal structure refinement of the target protein (Salmaso and Moro 2018). The structural coordinates of the inhibitor were completely removed from the protein inhibitor complex. Swiss-PDB Viewer was used for energy minimization by moving atoms to release local constraints for stability of the target protein. Different potential problems, such as missing side chains, missing atoms, missing bonds, molecule-chain breaks, added water, more than one molecule, alternate locations, and so on, were detected and fixed. Sufficient polar hydrogens were added and Kollman United Atom Charges were assigned to the target protein. Target protein was prepared in .pdbqt format for use in molecular docking studies.

Ligand preparation

Twenty-four circadian clock-modulating small molecules were selected based on their reported significant effect on the key components of the molecular circadian clock (for supporting references, refer Table 1). The 3D SDF files of all the small molecules were retrieved from the PubChem database (Table 1). SDF stands for structure-data file and is part of the family of chemical-data file format developed by MDL Information Systems, especially for structural information. All the small molecules were visualized in Discovery Studio Visualizer and were converted to ligand.pdb format. AutoDock tools accept files only in .pdb format. Therefore, the target and ligand must be converted into .pdb format. The PyRx tool (Dallakyan and Olson 2015) was used to prepare ligand as .pdbqt format for molecular docking.

Molecular docking

AutoDock Vina and MGL tools were used for the molecular docking studies (Trott and Olson 2010). Scaffolds

Table 1. Circadian clock-modulating small molecules used for docking with target protein SARS-CoV-2 M^{pro}.

S.No.	Small molecules	Description	Structure
1.	BRD1652 PubChem CID: 121237853 Molecular formula: $C_{20}H_{24}F_3N_3O$ IUPAC: (4 R)-4,7,7-trimethyl-4-phenyl-3-(trifluoromethyl)-1,2,3,3a,6,8,9,9a-octahydropyrazolo[3,4-b]quinolin-5-one.	GSK-3α inhibitor (Miller and Hirota 2020; Wagner et al. 2016)	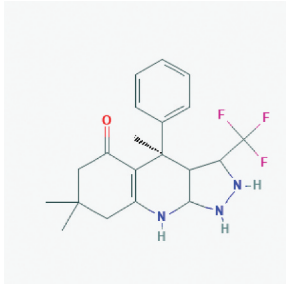
2.	CHIR99021 PubChem CID: 9956119 Molecular formula: $C_{22}H_{18}Cl_2N_8$ IUPAC: 6-[2-[[4-(2,4-dichlorophenyl)-5-(5-methyl-1 H-imidazol-2-yl)pyrimidin-2-yl]amino]ethylamino]pyridine-3-carbonitrile.	GSK-3α/β inhibitor (Ring et al. 2003)	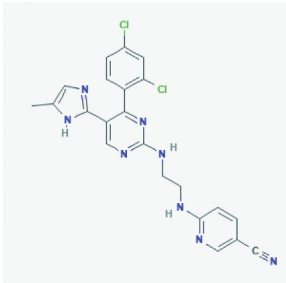
3.	CX-4945 PubChem CID: 24748573 Molecular formula: $C_{19}H_{12}ClN_3O_2$ IUPAC: 5-(3-chloroanilino)benzo[c][2,6]naphthyridine-8-carboxylic acid.	CK2 inhibitor (Miller and Hirota 2020; Siddiqui-Jain et al. 2010)	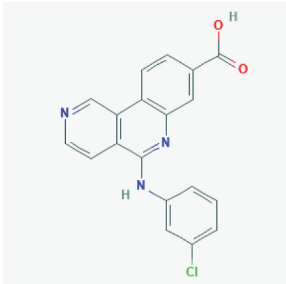
4.	DMAT PubChem CID: 5326976 Molecular formula: $C_9H_7Br_4N_3$ IUPAC: 4,5,6,7-tetrabromo-N,N-dimethyl-1 H-benzimidazol-2-amine.	CK2 inhibitor (Pagano et al. 2004)	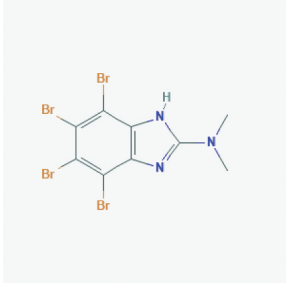
5.	EpiblastinA PubChem CID: 118987042 Molecular formula: $C_{12}H_{10}ClN_7$ IUPAC: 6-(3-chlorophenyl)pteridine-2,4,7-triamine.	CKIδ inhibitor (Ursu et al. 2016)	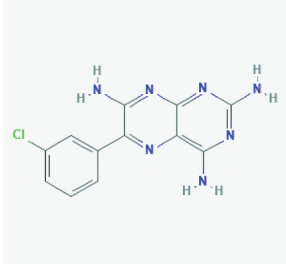

(*Continued*)

Table 1. (Continued).

S.No.	Small molecules	Description	Structure
6.	GSK2945 PubChem CID: 71682479 Molecular formula: $C_{20}H_{18}Cl_2N_2O_2S$ IUPAC:N-[(4-chloro-2-methylphenyl)methyl]-1-(4-chlorophenyl)-N-[(5-nitrothiophen-2-yl)methyl]methanamine.	REV-ERB agonist (Dierickx et al. 2019)	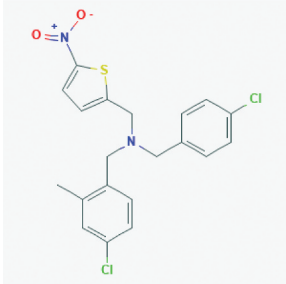
7.	GSK4112 PubChem CID: 50905018 Molecular formula: $C_{18}H_{21}ClN_2O_4S$ IUPAC: tert-butyl 2-[(4-chlorophenyl)methyl-[(5-nitrothiophen-2-yl)methyl] amino]acetate.	REV-ERB agonist (Meng et al. 2008)	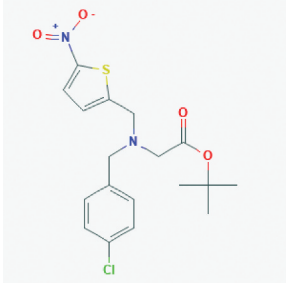
8.	KL044 PubChem CID: 91827381 Molecular formula: $C_{21}H_{14}ClN_3O$ IUPAC: 2-carbazol-9-yl-N-(2-chloro-6-cyanophenyl)acetamide.	CRY activator (Lee et al. 2015)	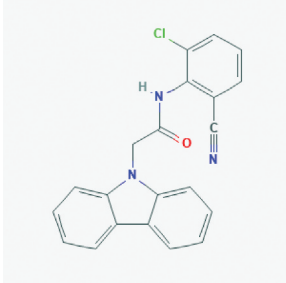
9.	Longdaysin PubChem CID: 49830252 Molecular formula: $C_{16}H_{16}F_3N_5$ IUPAC: 9-propan-2-yl-N-[[3-(trifluoromethyl)phenyl]methyl]purin-6-amine.	CKIα/δ inhibitor (Hirota et al. 2010; Miller and Hirota 2020)	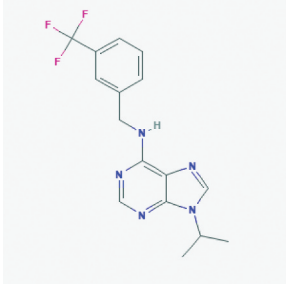
10.	NCC007 PubChem CID:138403252 Molecular formula: $C_{22}H_{28}F_3N_7$ IUPAC: 9-(1-cyclopropylethyl)-2-N-[2-(dimethylamino)ethyl]-6-N-[[3-(trifluoromethyl)phenyl] methyl]purine-2,6-diamine.	CKIα/δ inhibitor (Lee et al. 2019)	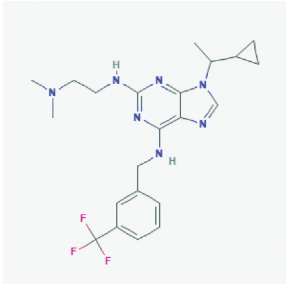

(*Continued*)

Table 1. (Continued).

S.No.	Small molecules	Description	Structure
11.	Neoruscogenin PubChem CID: 9910474 Molecular formula: $C_{27}H_{40}O_4$ IUPAC: (1S,2S,4S,6 R,7S,8 R,9S,12S,13 R,14 R,16 R)-7,9,13-trimethyl-5 -methylidenespiro[5-oxapentacyclo[10.8.0.02,9.04,8.013,18]icos-18-ene -6,2 -oxane]-14,16-diol.	RORα agonist (Helleboid et al. 2014)	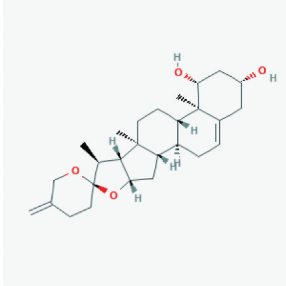
12.	Nobiletin PubChem CID: 72344 Molecular formula: $C_{21}H_{22}O_8$ IUPAC: 2-(3,4-dimethoxyphenyl)-5,6,7,8-tetramethoxychromen-4-one.	RORα/γ agonist (He et al. 2016)	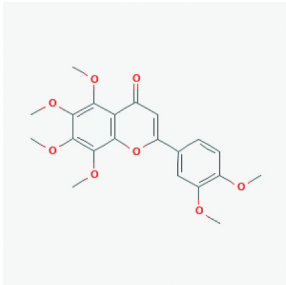
13.	PF670462 PubChem CID: 51049607 Molecular formula: $C_{19}H_{22}Cl_2FN_5$ IUPAC: 4-[3-cyclohexyl-5-(4-fluorophenyl)imidazol-4-yl]pyrimidin-2-amine; dihydrochloride.	CKIδ/ε inhibitor (Badura et al. 2007)	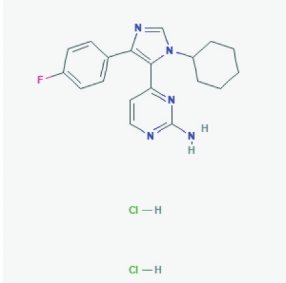
14.	PF4800567 PubChem CID: 53472153 Molecular formula: $C_{17}H_{18}ClN_5O_2$ IUPAC: 3-[(3-chlorophenoxy)methyl]-1-(oxan-4-yl)pyrazolo[3,4-d]pyrimidin-4-amine.	CK1ε inhibitor (Walton et al. 2009)	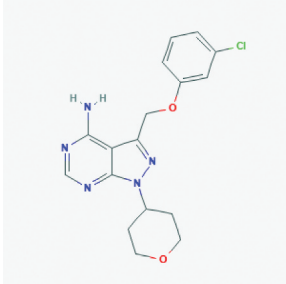
15.	SR1078 PubChem CID: 17980288 Molecular formula: $C_{17}H_{10}F_9NO_2$ IUPAC: N-[4-(1,1,1,3,3,3-hexafluoro-2-hydroxypropan-2-yl)phenyl]-4-(trifluoromethyl)benzamide.	ROR agonist (Wang et al. 2010)	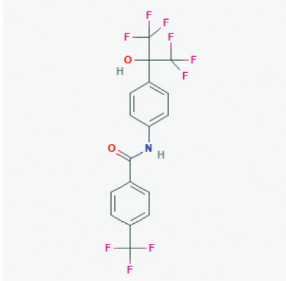

(*Continued*)

Table 1. (Continued).

S.No.	Small molecules	Description	Structure
16.	SR1001 PubChem CID: 44241473 Molecular formula: $C_{15}H_{13}F_6N_3O_4S_2$ IUPAC: N-[5-[[4-(1,1,1,3,3,3-hexafluoro-2-hydroxypropan-2-yl)phenyl] sulfamoyl]-4-methyl-1,3-thiazol-2-yl]acetamide.	RORα/γ inverse agonist (Solt et al. 2011)	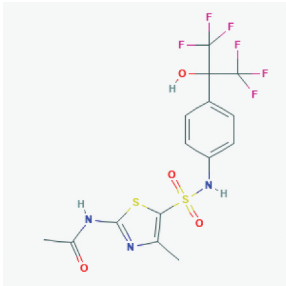
17.	SR3335 PubChem CID: 2360837 Molecular formula: $C_{13}H_9F_6NO_3S_2$ IUPAC: N-[4-(1,1,1,3,3,3-hexafluoro-2-hydroxypropan-2-yl)phenyl]thiophene-2-sulfonamide.	RORα inverse agonist (Kumar et al. 2011)	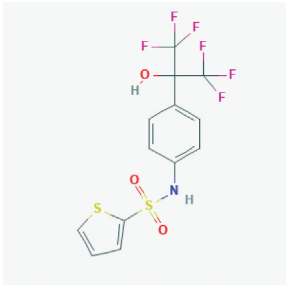
18.	SR9009 PubChem CID: 57394020 Molecular formula: $C_{20}H_{24}ClN_3O_4S$ IUPAC: ethyl 3-[[(4-chlorophenyl)methyl-[(5-nitrothiophen-2-yl)methyl]amino] methyl]pyrrolidine-1-carboxylate.	REV-ERB agonist (Solt et al. 2012)	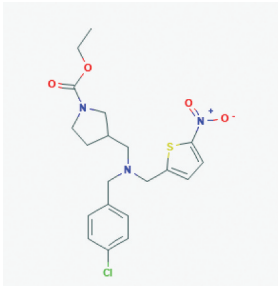
19.	SR8278 PubChem CID: 53393127 Molecular formula: $C_{18}H_{19}NO_3S_2$ IUPAC: ethyl 2-(5-methylsulfanylthiophene-2-carbonyl)-3,4-dihydro-1H-isoquinoline-3-carboxylate.	REV-ERB antagonist (Kojetin et al. 2011)	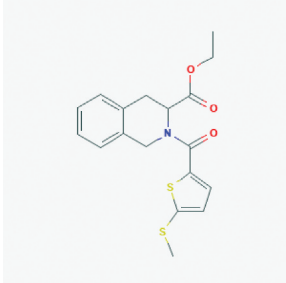
20.	SR10067 PubChem CID: 60168097 Molecular formula: $C_{31}H_{31}NO_3$ IUPAC: [3-[[4-[(2-methylpropan-2-yl)oxy]phenoxy]methyl]-3,4-dihydro-1H-isoquinolin-2-yl]-naphthalen-1-ylmethanone.	REV-ERB agonist (Banerjee et al. 2014)	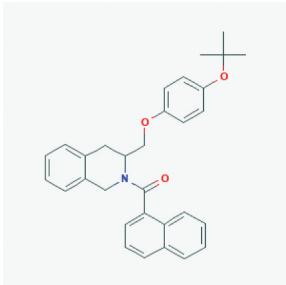

(*Continued*)

Table 1. (Continued).

S.No.	Small molecules	Description	Structure
21.	SRT1720 PubChem CID: 25232708 Molecular formula: $C_{25}H_{24}ClN_7OS$ IUPAC: N-[2-[3-(piperazin-1-ylmethyl)imidazo[2,1-b][1,3]thiazol-6-yl]phenyl] quinoxaline-2-carboxamide;hydrochloride.	SIRT1 agonist (Bellet et al. 2013; Sultan 2019)	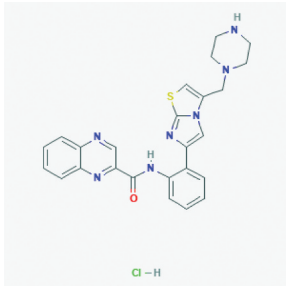
22.	SRT2183 PubChem CID: 24180126 Molecular formula: $C_{27}H_{24}N_4O_2S$ IUPAC: N-[2-[3-[[(3 R)-3-hydroxypyrrolidin-1-yl]methyl]imidazo[2,1-b][1,3] thiazol-6-yl]phenyl]naphthalene-2-carboxamide.	SIRT1 agonist (Bellet et al. 2013)	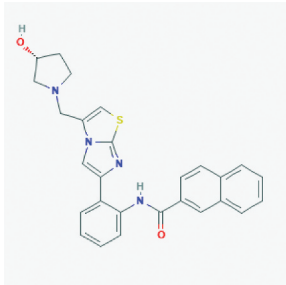
23.	T0901317 PubChem CID: 447912 Molecular formula: $C_{17}H_{12}F_9NO_3S$ IUPAC: N-[4-(1,1,1,3,3,3-hexafluoro-2-hydroxypropan-2-yl)phenyl]-N-(2,2,2-trifluoroethyl)benzenesulfonamide.	LXR agonist,RORα/γ inverse agonist (Kumar et al. 2010)	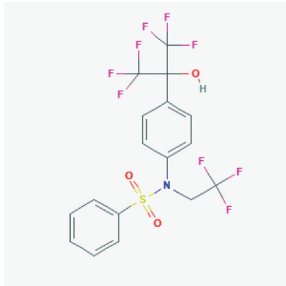
24.	TBB PubChem CID: 1694 Molecular formula: $C_6HBr_4N_3$ IUPAC: 4,5,6,7-tetrabromo-2H-benzotriazole.	CK2 inhibitor (Pagano et al. 2004)	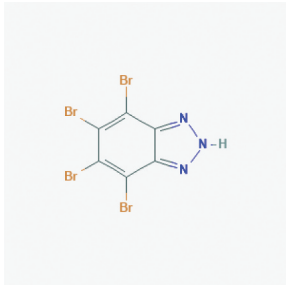

of circadian clock-modulating small molecules were blindly docked with the active sites of SARS-CoV-2 M^{pro}. The grid size for X, Y, and Z coordinates was 56, 70, and 66 Å, centralized at −26.60, 13.62, and 60.54, respectively. The grid spacing was 1.00 Å with the exhaustiveness of 8. Bound conformations, bonding interactions, and amino acid residues of the target protein binding to five proposed candidate small molecules were visualized and determined by PyMOL and Discovery Studio Visualizer. Polar interactions were mapped and labeled between the complexes. The charged potential was created on the target protein surface to decipher the binding of inhibitors in the deep groove of the target protein.

Inhibition constant (Ki; *nM*) calculation

Inhibition constant (*Ki;* nM) is an indicator of inhibiting potency; lower *Ki* value reflects higher potency of inhibitor. *Ki* was calculated from the ΔG (affinity describing the receptor–ligand interaction strength) using the formula:

$$Ki = \mathrm{EXP}\left((\Delta G * 1000) / (R * T)\right)$$

where ΔG = docking energy; R = 1.98719 cal K^{-1} $mol^{-1;T}$ $_{298.15°k}$

$$Ki = \mathrm{EXP}\left((A * 1000) / (198719 * 29815)\right).$$

Molecular dynamics (MD) simulation studies of SARS-CoV-2 M^{pro} and SARS-CoV-2 M^{pro} -SRT2183 complex

All-atom MD simulations were performed on SARS-CoV-2M^{pro} alone and in complex with ligand "SRT2183" (best ligand sorted on the basis of binding free energy and ligand–protein interactions) to determine conformational dynamics in the aqueous environment. The trajectories of the SARS-CoV-2 M^{pro} and SARS-CoV-2 M^{pro}-SRT2183 complex were studied through 50 ns of MD simulations at 300 K using GROMOS96 force-field in GROMACS 5.1.2. The topology files of the SRT2183 were computed using PRODRG server (an external web plate form). Topology files of SRT2183 were merged with the protein topology to generate the SARS-CoV-2 M^{pro}-SRT2183 complex system. Both systems were solvated in a cubic box with the Simple Point Charge (spc216) water model to simulate aqueous surroundings (Goel et al. 2011; Lagunin et al. 2000). Both systems were subjected to energy minimization using 1500 steps of the steepest descent method for 100 ps to remove their possible steric clashes. The temperature of both systems was subsequently increased from 0 to 300 K during the equilibration period of 100 ps at a constant volume under periodic boundary conditions with a stable environment of 1-bar pressure. Various geometrical properties of the systems, such as root-mean-square deviation (RMSD), root-mean-square fluctuation (RMSF), radius of gyration (Rg), and solvent accessible surface area (SASA), were determined using g_rmsd, g_rmsf, g_gyrate, and g_sas programs. All the graphs were plotted using Xmgrace tool.

MM-PBSA calculation

Molecular mechanics Poisson–Boltzmann surface area (MM-PBSA) is a method to estimate interaction free energies (Kumari et al. 2014). It has been increasingly used in the study of biomolecular interactions. The MM-PBSA calculations were performed using MD scripts (Bhardwaj et al. 2020). The MM-PBSA binding free energies were calculated using g_mmpbsa script of GROMACS (Kumari et al. 2014). The following equation was implemented for the calculation of binding energy:

$$\Delta G_{binding} = G_{complex} - \left(G_{receptor} + G_{ligand}\right)$$

where $\Delta G_{binding}$ represents the total binding energy of the protein-ligand complex, $G_{receptor}$ represents the binding energy of free receptor, and G_{ligand} represents the binding energy of the unbounded ligand.

Result and discussion

Global health emergency is warranting the development of targeted therapy for the treatment and control of the newly emerged coronavirus disease COVID-19. Identification and development of targeted therapeutic agents are vigorously being pursued against different target molecules, particularly SARS-CoV-2 M^{pro}. Using a structure-assisted drug designing approach, many inhibitor molecules of M^{pro} have been proposed for the therapeutic management of COVID-19 (Jin et al. 2020a, 2020b; McKee et al. 2020; Wang et al. 2020; Zhang et al. 2001). Only few have shown inhibition potency in bioassays. These findings warrant identifying and developing more compelling inhibitors against SARS-CoV-2 M^{pro} for the therapeutic management of COVID-19.

In the present study, 24 circadian clock-modulating small molecules (presented in Table 1) were blindly docked against the target molecule "SARS-CoV-2 M^{pro}." These molecules were ranked according to their binding energy values (presented in Table 2). Based on the high binding affinity values (more than −8.0 Kcal/Mol), we present five molecules; SRT2183, Neoruscogenin, SR10067, SRT1720, and CX-4945 as potent inhibitors of SARS-CoV-2 M^{pro} (Table 2). The higher binding affinity values of these five molecules reflect their likelihood for the inhibition of SARS-CoV-2 M^{pro} to block replication and spread. These five small molecules were subjected to further analysis to explore the best docking pose on the target protein surface. Protein-inhibitor complexes reflected that all the five inhibitor molecules bind in the deep grove and occupied substrate-binding sites on the target protein.

Previous studies have shown that M^{pro} forms a homodimer with three domains (domain I (residues 10–99), II (residues 100–184), and III (residues 201–303)) in each monomer (Jin et al. 2020a, 2020b; Lu et al. 2006; Wu et al. 2020a). In addition, amino

Table 2. Binding affinities and inhibition constant (*Ki*) of circadian clock-modulating small molecules with target protein SARS-CoV-2 $M^{pro.}$

S.No.	Small molecules	Target protein	Binding affinity (Kcal/Mol)	Inhibition constant, *Ki* (nM)
1.	BRD1652	SARS-CoV-2 M^{pro}	−7.8	1.91655E-06
2.	CHIR99021		−7.0	7.39482E-06
3.	CX-4945		−8.3	8.24165E-07
4.	DMAT		−5.1	0.000182662
5.	Epiblastin A		−7.1	6.24635E-06
6.	GSK4112		−6.6	1.45255E-05
7.	GSK2945		−7.1	6.24635E-06
8.	KL044		−7.6	2.6861E-06
9.	Longdaysin		−7.0	7.39482E-06
10.	NCC007		−7.2	5.27625E-06
11.	Neoruscogenin		−8.5	5.88047E-07
12.	Nobiletin		−6.4	2.03579E-05
13.	PF670462		−7.0	7.39482E-06
14.	PF4800567		−7.2	5.27625E-06
15.	SR1078		−7.9	1.61889E-06
16.	SR1001		−7.8	1.91655E-06
17.	SR3335		−7.0	7.39482E-06
18.	SR9009		−7.0	7.39482E-06
19.	SR8278		−7.2	5.27625E-06
20.	SR10067		−8.4	6.96166E-07
21.	SRT1720		−8.4	6.96166E-07
22.	SRT2183		−9.2	1.80428E-07
23.	T0901317		−7.4	3.76464E-06
24.	TBB		−6.0	3.99888E-05

acid residues 185–200 form a long loop that connects domains II and III together (Jin et al. 2020a, 2020b). It has been reported that catalytic dyad residues are present in the region between domains I and II (Wu et al. 2020a). Here, we present docked protein-inhibitor complexes for all the five selected small molecules (Figures 1a, 2a, 3a, 4a, and 5a). Analysis of these complexes revealed that these proposed inhibitor molecules bind in a region mapped between domains I and II of the monomer. Surface representation of the complexes reflected a strong binding pattern of each inhibitor in the main groove of the target protein (Figures 1b, 2b, 3b, 4b, and 5b). These results indicate that blocking the catalytic site may highly affect the M^{pro} activity leading to cessation of viral replication (Lu et al. 2006).

Next, protein-inhibitor complexes were analyzed to uncover the residual interaction and bonding of M^{pro} with selected inhibitor molecules. Results showed that SRT2183 formed major interactions with PHE294, GLN110, VAL202, PRO293, VAL297, PRO252, and ILE249 (Figure 1c and d), Neoruscogenin with LEU286, LEU287 and LYS137 (Figure 2c and d), SR10067 with ASP153, PHE294, ASN151, PRO293, ILE249, and VAL104 (Figure 3c and d), SRT1720 with ILE249, PRO293, VAL202, GLN110, and PHE294 (Figure 4c and d), and CX-4945 with ASP295, PHE294, PRO293, ILE249, and THR111 (Figure 5c and d) amino acid residues of the target protein. In addition to these major interactions, sub-interactions were also formed by these molecules with amino acid residues of M^{pro}. These amino acid residues are presented in Table 3 and Figures 1c, 2c, 3c, 4c, and 5c. The majority of these amino acid residues have been reported to provide plinth for the binding of potent inhibitors of M^{pro} aimed to be developed as therapeutic agents for the management and control of contagious coronavirus diseases (Jin et al. 2020a, 2020b; Zhang et al. 2020). Moreover, the results showed that protein-inhibitor complexes involved the formation of different types of bonds (Figures 1c, 2c, 3c, 4c, and 5c). Many common type of bonding interactions were formed by these molecules with the M^{pro}. These bonding interactions are likely to contribute to sturdy binding of inhibitors with the target protein M^{pro} (Jo et al. 2020; Zhang et al. 2020).

Among these top five candidate small molecules, the best ligand "SRT2183" was sorted on the basis of

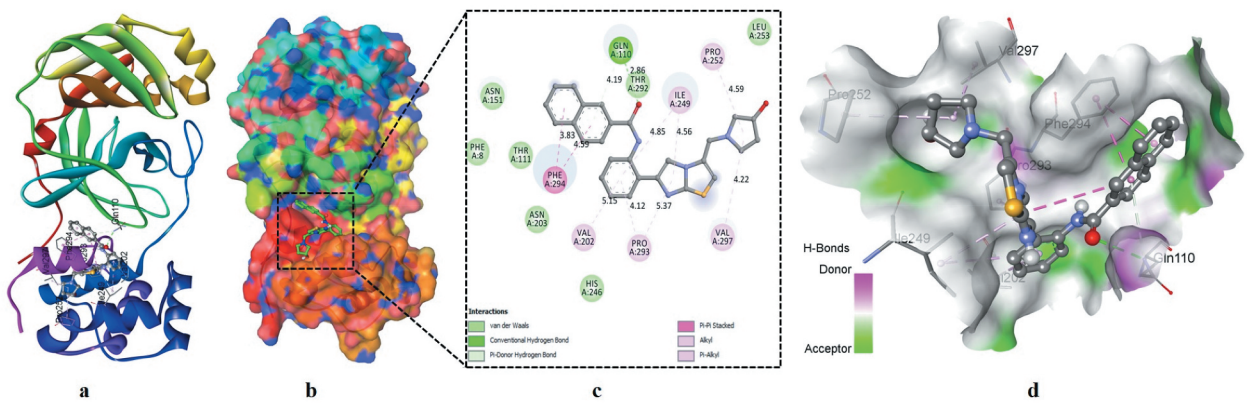

Figure 1. The crystal structure of SARS-CoV-2 M^{pro} in complex with SRT2183. (a) A cartoon presentation of M^{pro}-inhibitor complex. (b) Surface presentation of M^{pro}. SRT2183 is presented in green color sticks. (c) A zoomed view of substrate-binding pocket representing the key amino acid residues forming interactions with inhibitor molecule. (d) Surface presentation of conserved substrate-binding pocket of SARS-CoV-2 M^{pro}.

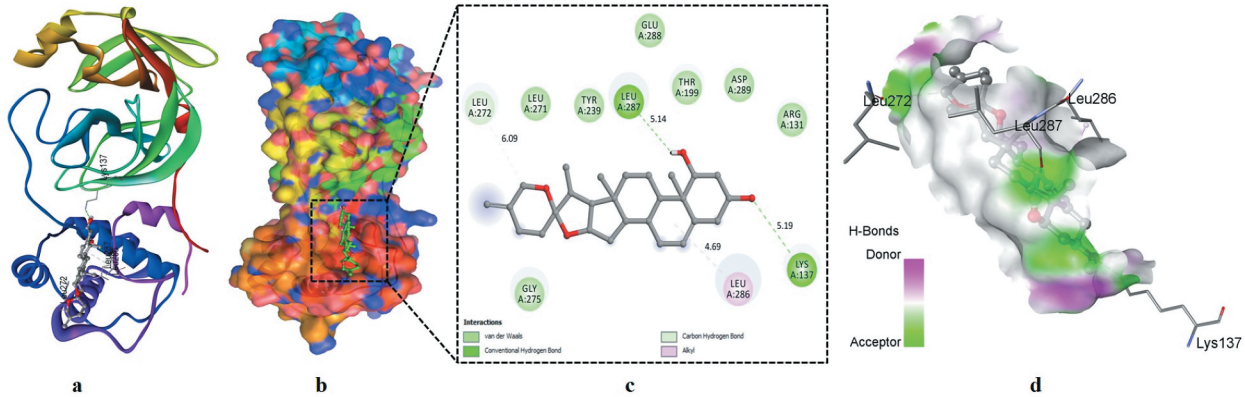

Figure 2. The crystal structure of SARS-CoV-2 M^{pro} in complex with Neoruscogenin. (a) A cartoon presentation of M^{pro}-inhibitor complex. (b) Surface presentation of M^{pro}. Neoruscogenin is presented in green color sticks. (c) A zoomed view of substrate-binding pocket representing the key amino acid residues forming interactions with inhibitor molecule. (d) Surface presentation of conserved substrate-binding pocket of SARS-CoV-2 M^{pro}.

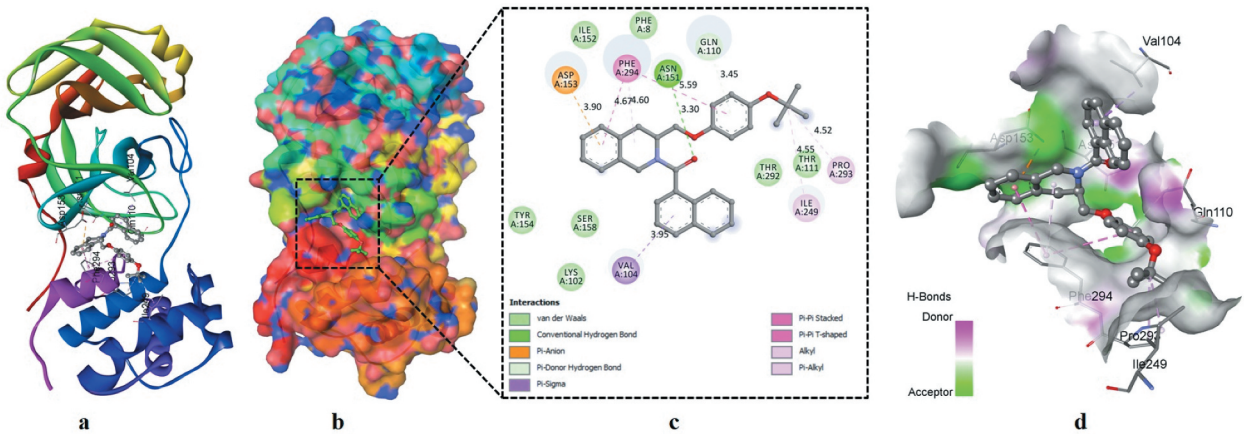

Figure 3. The crystal structure of SARS-CoV-2 M^{pro} in complex with SR10067. (a) A cartoon presentation of M^{pro}-inhibitor complex. (b) Surface presentation of M^{pro}. SR10067 is presented in green color sticks. (c) A zoomed view of substrate-binding pocket representing the key amino acid residues forming interactions with inhibitor molecule. (d) Surface presentation of conserved substrate-binding pocket of SARS-CoV-2 M^{pro}.

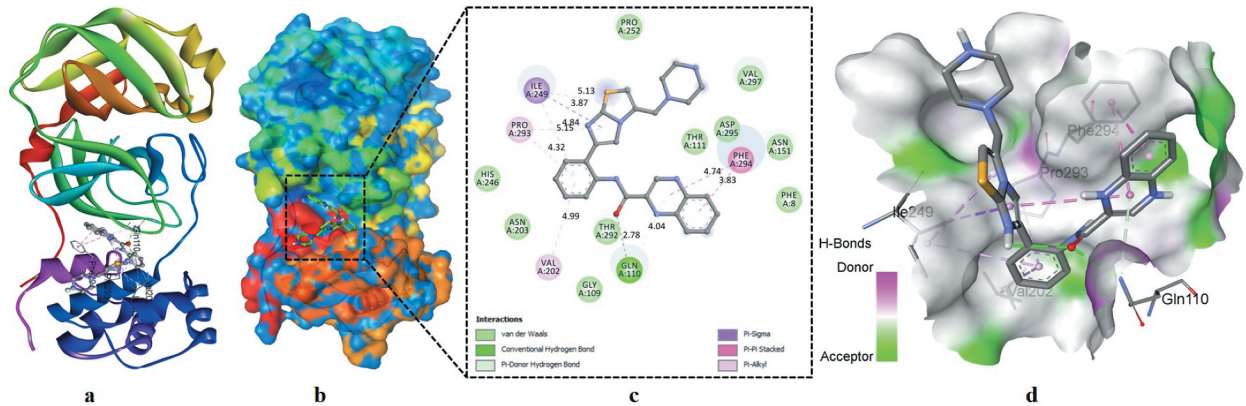

Figure 4. The crystal structure of SARS-CoV-2 M^{pro} in complex with SRT1720. (a) A cartoon presentation of M^{pro}-inhibitor complex. (b) Surface presentation of M^{pro}. SRT1720 is presented in green color sticks. (c) A zoomed view of substrate-binding pocket representing the key amino acid residues forming interactions with inhibitor molecule. (d) Surface presentation of conserved substrate-binding pocket of SARS-CoV-2 M^{pro}.

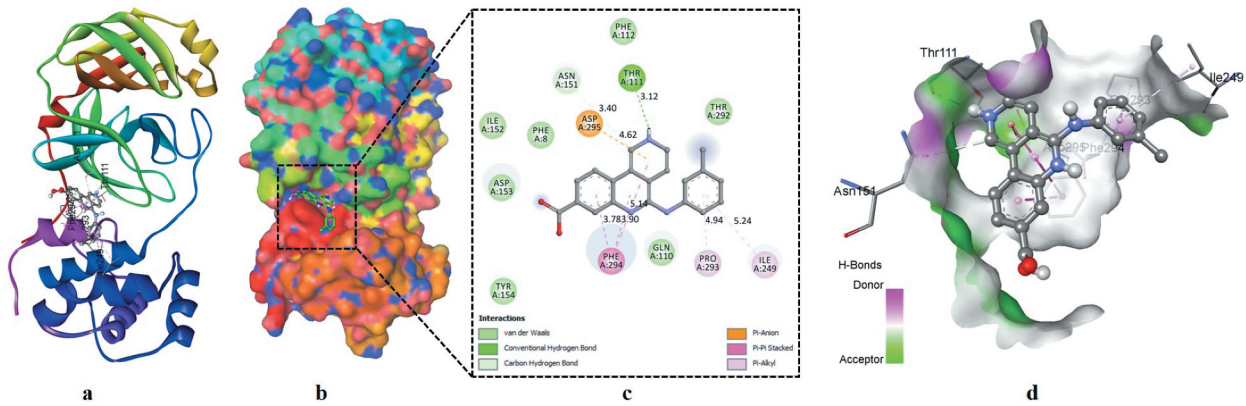

Figure 5. The crystal structure of SARS-CoV-2 M^{pro} in complex with CX-4945. (a) A cartoon presentation of M^{pro}-inhibitor complex. (b) Surface presentation of M^{pro}. CX-4945 is presented in green color sticks. (c) A zoomed view of substrate-binding pocket representing the key amino acid residues forming interactions with inhibitor molecule. (d) Surface presentation of conserved substrate-binding pocket of SARS-CoV-2 M^{pro}.

Table 3. Interacting amino acid residues of target protein SARS-CoV-2 M^{pro} with five proposed circadian clock-modulating small molecules as its potent inhibitors.

S. No.	Small molecules	Target protein	Integrating amino acid residues
1.	SRT2183	SARS-CoV-2 M^{pro}	GLN110, PRO252, ILE249, VAL297, PRO293, VAL202, PHE294, LEU253, THR292, ASN151, PHE8, THR111, ASN203, HIS246.
2.	Neoruscogenin		LEU287, LYS137, LEU272, LEU286, GLY275, LEU271, TYR239, GLU288, THR199, ASP289, ARG131.
3.	SR10067		ASN151, GLN110, PHE294, ASP153, VAL104, ILE249, PRO293, ILE152, PHE8, TYR154, SER158, LYS102, THR292, THR111.
4.	SRT1720		GLN110, VAL202, PRO293, ILE249, PHE294, PRO252, HIS246, ASN203, THR292, GLY109, PHE8, ASN151, ASP295, THR111, VAL297.
5.	CX-4945		THR111, ASN151, ASP295, PHE294, PRO293, ILE249, THR292, PHE112, PHE8, ILE152, ASP153, TYR154, GLN110.

highest-binding affinity (−9.2 Kcal/mol). Thereafter, all-atom MD simulations (50 ns) were performed on the target protein "SARS-CoV-2 M^{pro}" alone and in complex with ligand "SRT2183" to determine conformational dynamics in an aqueous environment. Average values of RMSD, RMSF, radius of gyration (Rg), and solvent accessible surface area (SASA) along with kinetic energy, enthalpy, volume, potential energy, and density of the systems are presented in Table 4. It is well known that binding of any ligand induces conformational changes in the native structure of the target protein (Seo et al. 2014). Degrees of conformational changes are quantified by calculating the RMSD with time from the MD simulation generated data (Kuzmanic and Zagrovic 2010). RMSD plots of the SARS-CoV-2 M^{pro} and SARS-CoV-2 M^{pro}-SRT2183 complex are presented as Figure 6a. Average RMSD values for SARS-CoV-2M^{pro} and SARS-CoV-2 M^{pro}-SRT2183 complex were found 0.323616 and 0.325814 nm, respectively (Table 4). Initially, RMSD plots of SARS-CoV-2 M^{pro} and SARS-CoV-2 M^{pro}-SRT2183 complex reflected distinct fashion of deviation until 05 ns due to their initial orientation. Despite the initial structural arrangements of the docked complex, the average RMSD of the trajectories for bound protein backbone atoms showed equilibration and stabilization throughout the 50 ns MD simulations, reflecting no large conformational change in the native conformation of SARS-CoV-2 M^{pro} and confirming the stability of the SARS-CoV-2 M^{pro}-SRT2183 complex (Bello et al. 2020). Local protein mobility was analyzed by measuring the time-averaged RMSF value of SARS-CoV-2 M^{pro} and SARS-CoV-2 M^{pro}-SRT2183 complex against residue numbers based on trajectory data (Kuzmanic and Zagrovic 2010; Yadav et al. 2018).

Table 4. Parameters calculated for both the systems obtained after 50 ns MD simulations.

	Average RMSD (nm)	Average RMSF (nm)	Average *Rg* (nm)	Average SASA (nm^2)	Kinetic Energy kJ/mol	Enthalpy kJ/mol	Volume (nm^3)	Potential energy kJ/mol	Density (kg/m^3)
SARS-CoV-2 M^{pro}	0.323616	0.168463	2.14602	134.6	229233	−118960	927.87	−1418890	1015.91
SARS-CoV-2 M^{pro}-SRT2183 complex	0.325814	0.189153	2.15737	136.1	159964	−722497	664.01	−882501	1003.13

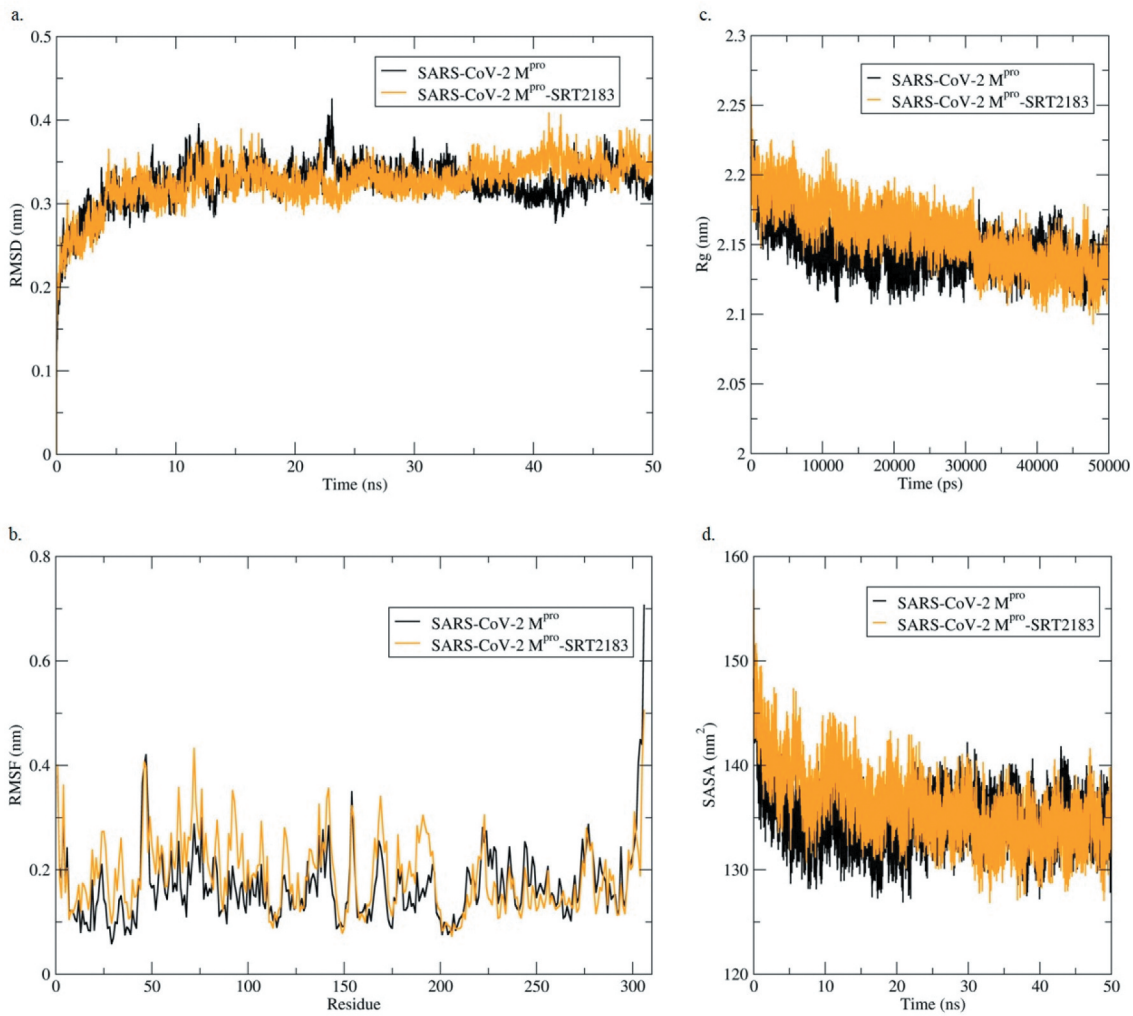

Figure 6. (a) Root-mean-square deviation (RMSD) for saquinavir in complex with SARS-CoV-2 M^{pro}; (b) Root-mean-square fluctuations (RMSF) for saquinavir in complex with SARS-CoV-2 M^{pro}; (c) Time evolution of the radius of gyration (Rg) for saquinavir in complex with SARS-CoV-2 M^{pro}; (d) Solvent accessible surface area (SASA) for saquinavir in complex with SARS-CoV-2 M^{pro}.

RMSF plot is presented as Figure 6b. Average RMSF measured for SARS-CoV-2 M^{pro} and SARS-CoV-2 M^{pro}-SRT2183 complex were 0.168463 nm and 0.189153 nm, respectively, reflecting the relative stability of the complex in its favorable conformations for inhibition. Next, we determined the Rg values for SARS-CoV -2 M^{pro} alone and in complex with SRT2183. The Rg provides information about the overall dimension and the shape of the protein (Yadav et al. 2018). The Rg values for SARS-CoV-2 M^{pro} and SARS-CoV-2 M^{pro}-SRT2183 complex were 2.14602 nm and 2.15737 nm, respectively. These Rg values indicate that the overall shape of the protein is stable upon binding of the ligand (Yadav et al. 2018). Further, we computed the SASA of SARS-CoV-2M^{pro} and SARS-CoV-2 M^{pro}-SRT2183 complex to investigate their conformational behavior during the simulation. SASA calculations provide insight regarding the interface between a protein and its surrounding solvent due to its electrostatic and surface properties, reflecting their conformational behavior during the simulation (Rodier et al. 2005). The values of average SASA for SARS-CoV-2 M^{pro} and SARS-CoV-2 M^{pro}-SRT2183 complex were found 134.6 nm^2 and 136.1 nm^2, respectively. A small increment in SASA was observed in the complex, possibly due to the increased surface area of SARS-CoV-2 M^{pro} in the presence of SRT2183, where some inner residues might be exposed to the surface (Figure 6d). The SASA attained stable equilibrium without switching throughout the simulation, thus suggesting the structural stability of SARS-CoV-2 Mpro in the presence of compound SRT2183.

We also computed the binding free energy for SARS-CoV-2 M^{pro}-SRT2183 complex by implementing MM-PBSA calculations. The energy liberated during the process of bond formation, or alternatively, the interaction between

Table 5. MM-PBSA calculations of binding free energy for SARS-CoV-2 M^{pro}-SRT2183 complex.

Complex	$\Delta E_{binding\ (kj/mol)}$	SASA (kJ/mol)	$\Delta E_{polar\ solvation\ (kj/mol)}$	$\Delta E_{Electrostatic\ (kj/mol)}$	$\Delta E_{Van\ der\ Waal\ (kj/mol)}$
SARS-CoV-2 M^{pro}- SRT2183 complex	−210.517 ± 16.215	−22.775 ± 1.759	139.657 ± 17.275	−51.868 ± 13.417	−269.316 ± 18.612

a ligand and protein is shown in the form of binding energy (Bhardwaj et al. 2020). Lesser binding energy reflects better binding between ligand and protein. The final binding energy is the cumulative sum of electrostatic, polar solvation, van der Wall, and SASA energy (Bhardwaj et al. 2020). The values of average free binding energy and its standard deviations are presented in Table 5. The results reflect that all forms of energy contributed constructively to the interaction between SARS-CoV-2 M^{pro} and SRT2183.

In conclusion, the present study reported circadian clock-modulating small molecule "SRT2183" as potent inhibitor of M^{pro}. To validate these preliminary findings, binding studies and bioassays are warranted using this potent inhibitor against purified M^{pro} protein. Targeting and inhibiting the activity of this enzyme may lead to the discovery of a potent therapeutic agent for the treatment and control of COVID-19 pandemic.

Acknowledgements

Department of Biotechnology (DBT), India is highly acknowledged for providing fellowship to AS working as Research Associate. SA is grateful to SERB-DST, India for the award of JC Bose National Fellowship (SR/S2/JCB-49/2011) and to the Department of Biotechnology (DBT), Government of India (BT/PR12828/AAQ/1/622/2015) for financial support.

ORCID

Armiya Sultan http://orcid.org/0000-0001-5373-8824
Rafat Ali http://orcid.org/0000-0001-6324-7236
Arti Parganiha http://orcid.org/0000-0001-9764-5566

Declaration of Interest

The authors report no conflict of interest.

References

Badura L, Swanson T, Adamowicz W, Adams J, Cianfrogna J, Fisher K, Holland J, Kleiman R, Nelson F, Reynolds L, et al. 2007. An inhibitor of casein kinase I epsilon induces phase delays in circadian rhythms under free-running and entrained conditions. J Pharmacol Exp Ther. 322 (2):730–738. doi:10.1124/jpet.107.122846.

Banerjee S, Wang Y, Solt LA, Griffett K, Kazantzis M, Amador A, El-Gendy BM, Huitron-Resendiz S, Roberts AJ, Shin Y, et al. 2014. Pharmacological targeting of the mammalian clock regulates sleep architecture and emotional behaviour. Nat Commun. 5:5759. doi:10.1038/ncomms6759.

Bellet MM, Nakahata Y, Boudjelal M, Watts E, Mossakowska DE, Edwards KA, Cervantes M, Astarita G, Loh C, Ellis JL, et al. 2013. Pharmacological modulation of circadian rhythms by synthetic activators of the deacetylase SIRT1. Proc Natl Acad Sci USA. 110(9):3333–3338. doi:10.1073/pnas.1214266110.

Bello M, Martínez-Muñoz A, Balbuena-Rebolledo I. 2020. Identification of saquinavir as a potent inhibitor of dimeric SARS-CoV2 main protease through MM/GBSA. J Mol Model. 26(12):340. doi:10.1007/s00894-020-04600-4.

Bhardwaj VK, Singh R, Sharma J, Rajendran V, Purohit R, Kumar S. 2020. Identification of bioactive molecules from tea plant as SARS-CoV-2 main protease inhibitors. J Biomol Struct Dyn. doi:10.1080/07391102.2020.1766572.

Chen N, Zhou M, Dong X, Qu J, Gong F, Han Y, Qiu Y, Wang J, Liu Y, Wei Y, et al. 2020. Epidemiological and clinical characteristics of 99 cases of 2019 novel coronavirus pneumonia in Wuhan, China: a descriptive study. Lancet. 395(10223):507–513. doi:10.1016/S0140-6736(20)30211-7.

Chowdhury S, Sripathy S, Webster A, Park A, Lao U, Hsu JH, Loe T, Bedalov A, Simon JA. 2020. Discovery of selective SIRT2 inhibitors as therapeutic agents in B-cell lymphoma and other malignancies. Molecules. 21;25(3):455. doi:10.3390/molecules25030455.

Dallakyan S, Olson AJ. 2015. Small-molecule library screening by docking with PyRx. Methods Mol Biol. 1263:243–250. doi:10.1007/978-1-4939-2269-7_19.

Dierickx P, Emmett MJ, Jiang C, Uehara K, Liu M, Adlanmerini M, Lazar MA. 2019. SR9009 has REV-ERB-independent effects on cell proliferation and metabolism. Proc Natl Acad Sci USA. 116(25):12147–12152. doi:10.1073/pnas.1904226116.

Goel RK, Singh D, Lagunin A, Poroikov V. 2011. PASS-assisted exploration of new therapeutic potential of natural products. Med Chem Res. 20:1509–1514. doi:10.1007/s00044-010-9398-y.

Gorbalenya AE, Baker SC, Baric RS, De Groot RJ, Drosten C, Gulyaeva AA, Haagmans BL, Lauber C, Leontovich AM, Neuman BW, et al. 2020. The species severe acute respiratory syndrome-related coronavirus: classifying 2019-nCoV and naming it SARS-CoV-2. Nat Microbiol. 5:536–544. doi:10.1038/s41564-020-0695-z.

He B, Nohara K, Park N, Park YS, Guillory B, Zhao Z, Garcia JM, Koike N, Lee CC, Takahashi JS, et al. 2016. The small molecule nobiletin targets the molecular oscillator to enhance circadian rhythms and protect against metabolic syndrome. Cell Metab. 23(4):610–621. doi:10.1016/j.cmet.2016.03.007.

Hegyi A, Ziebuhr J. 2002. Conservation of substrate specificities among coronavirus main proteases. J Gen Virol. 83:595–599. doi:10.1099/0022-1317-83-3-595.

Helleboid S, Haug C, Lamottke K, Zhou Y, Wei J, Daix S, Cambula L, Rigou G, Hum DW, Walczak R. 2014. The identification of naturally occurring neoruscogenin as a bioavailable, potent, and high-affinity agonist of the nuclear receptor RORα (NR1F1). J Biomol Screen. 19 (3):399–406. doi:10.1177/1087057113497095.

Hirota T, Lee JW, Lewis WG, Zhang EE, Breton G, Liu X, Garcia M, Peters EC, Etchegaray JP, Traver D, et al. 2010.

High-throughput chemical screen identifies a novel potent modulator of cellular circadian rhythms and reveals CKIα as a clock regulatory kinase. PLoS Biol. 8(12):e1000559. doi:10.1371/journal.pbio.1000559.

Jin Z, Du X, Xu Y, Deng Y, Liu M, Zhao Y, Zhang B, Li X, Zhang L, Peng C, et al. 2020a. Structure of Mpro from SARS-CoV-2 and discovery of its inhibitors. Nature. 582 (7811):289–293. doi:10.1038/s41586-020-2223-y.

Jin Z, Zhao Y, Sun Y, Zhang B, Wang H, Wu Y, Zhu Y, Zhu C, Hu T, Du X, et al. 2020b. Structural basis for the inhibition of SARS-CoV-2 main protease by antineoplastic drug carmofur. Nat Struct Mol Biol. 27(6):529–532. doi:10.1038/s41594-020-0440-6.

Jo S, Kim S, Shin DH, Kim MS. 2020. Inhibition of SARS-CoV 3CL protease by flavonoids. J Enzyme Inhib Med Chem. 35 (1):145–151. doi:10.1080/14756366.2019.1690480.

Kim HM, Jeong I, Kim HJ, Kang SK, Kwon WS, Kim TS, Park KH, Jung M, Soong J, Lin SC, et al. 2018. Casein kinase 2 inhibitor, CX-4945, as a potential targeted anticancer agent in gastric cancer. Anticancer Res. 38(11):6171–6180. doi:10.21873/anticanres.12970.

Kojetin D, Wang Y, Kamenecka TM, Burris TP. 2011. Identification of SR8278, a synthetic antagonist of the nuclear heme receptor REV-ERB. ACS Chem Biol. 6 (2):131–134. doi:10.1021/cb1002575.

Kumar N, Kojetin DJ, Solt LA, Kumar KG, Nuhant P, Duckett DR, Cameron MD, Butler AA, Roush WR, Griffin PR, et al. 2011. Identification of SR3335 (ML176): a synthetic RORa selective inverse agonist. ACS Chem Biol. 6:218e222. doi:10.1021/cb1002762.

Kumar N, Solt LA, Conkright JJ, Wang Y, Istrate MA, Busby SA, Garcia-Ordonez RD, Burris TP, Griffin PR. 2010. The benzenesulfoamide T0901317 [N-(2,2,2-trifluoroethyl)-N-[4-[2,2,2-trifluoro-1-hydroxy-1-(trifluoromethyl)ethyl]phenyl]-benzenesulfonamide] is a novel retinoic acid receptor-related orphan receptor-alpha/gamma inverse agonist. Mol Pharmacol. 77(2):228–236. doi:10.1124/mol.109.060905.

Kumari R, Kumar R, Open Source Drug Discovery Consortium, Lynn A. 2014. g_mmpbsa-a GROMACS tool for high-throughput MM-PBSA calculations. J ChemInf Model. 54(7):1951–1962. doi:10.1021/ci500020m.

Kuzmanic A, Zagrovic B. 2010. Determination of ensemble-average pairwise root mean-square deviation from experimental B-factors. Biophys J. 98(5):861–871. doi:10.1016/j.bpj.2009.11.011.

Lagunin A, Stepanchikova A, Filimonov D, Poroikov V. 2000. PASS: prediction of activity spectra for biologically active substances. Bioinformatics. 16(8):747–748. doi:10.1093/bioinformatics/16.8.747.

Lahusen TJ, Deng CX. 2015. SRT1720 induces lysosomal-dependent cell death of breast cancer cells. Mol Cancer Ther. 14 (1):183–192. doi:10.1158/1535-7163.MCT-14-0584.

Lee JW, Hirota T, Kumar A, Kim NJ, Irle S, Kay SA. 2015. Development of small-molecule cryptochrome stabilizer derivatives as modulators of the circadian clock. Chem Med Chem. 10(9):1489–1497. doi:10.1002/cmdc.201500260.

Lee JW, Hirota T, Ono D, Honma S, Honma KI, Park K, Kay SA. 2019. Chemical control of mammalian circadian behavior through dual inhibition of casein kinase Iα and δ. J Med Chem. 62(4):1989–1998. doi:10.1021/acs.jmedchem.8b01541.

Li Q, Guan X, Wu P, Wang X, Zhou L, Tong Y, Ren R, Leung KSM, Lau EHY, Wong JY, et al. 2020. Early transmission dynamics in Wuhan, China, of novel coronavirus-infected pneumonia. N Engl J Med. 382 (13):1199–1207. doi:10.1056/NEJMoa2001316.

Lu IL, Mahindroo N, Liang PH, Peng YH, Kuo CJ, Tsai KC, Hsieh HP, Chao YS, Wu SY. 2006. Structure-based drug design and structural biology study of novel nonpeptide inhibitors of severe acute respiratory syndrome coronavirus main protease. J Med Chem. 49(17):5154–5161. doi:10.1021/jm060207o.

Mazzoccoli G, Vinciguerra M, Carbone A, Relógio A. 2020. The circadian clock, the immune system, and viral infections: the intricate relationship between biological time and host-virus interaction. Pathogens. 9(2):83. doi:10.3390/pathogens9020083.

McKee DL, Sternberg A, Stange U, Laufer S, Naujokat C. 2020. Candidate drugs against SARS-CoV-2 and COVID-19. Pharmacol Res. 157:104859. doi:10.1016/j.phrs.2020.104859.

Meng QJ, McMaster A, Beesley S, Lu WQ, Gibbs J, Parks D, Collins J, Farrow S, Donn R, Ray D, et al. 2008. Ligand modulation of REV-ERBalpha function resets the peripheral circadian clock in a phasic manner. J Cell Sci. 121(Pt 21):3629–3635. doi:10.1242/jcs.035048.

Miller S, Hirota T. 2020. Pharmacological interventions to circadian clocks and their molecular bases. J Mol Biol. 432 (12):3498–3514. doi:10.1016/j.jmb.2020.01.003.

Pagano MA, Meggio F, Ruzzene M, Andrzejewska M, Kazimierczuk Z, Pinna LA. 2004. 2-Dimethylamino-4,5,6,7-tetrabromo-1H-benzimidazole: a novel powerful and selective inhibitor of protein kinase CK2. Biochem Biophys Res Commun. 321(4):1040–1044. doi:10.1016/j.bbrc.2004.07.067.

Palliyaguru DL, Minor RK, Mitchell SJ, Palacios HH, Licata JJ, Ward TM, Abulwerdi G, Elliott P, Westphal C, Ellis JL, et al. 2020. Combining a high dose of metformin with the SIRT1 activator, SRT1720, reduces life span in aged mice fed a high-fat diet. J Gerontol A Biol Sci Med Sci. 75 (11):2037–2041. doi:10.1093/gerona/glaa148.

Pillaiyar T. 2016. An overview of severe acute respiratory syndrome-coronavirus (SARS-CoV) 3CL protease inhibitors: peptidomimetics and small molecule chemotherapy. J Med Chem. 59:6595–6628. doi:10.1021/acs.jmedchem.5b01461.

Ray S, Reddy AB. 2020. COVID-19 management in light of the circadian clock. Nat Rev Mol Cell Biol. 21(9):494–495. doi:10.1038/s41580-020-0275-3.

Ring DB, Johnson KW, Henriksen EJ, Nuss JM, Goff D, Kinnick TR, Ma ST, Reeder JW, Samuels I, Slabiak T, et al. 2003. Selective glycogen synthase kinase 3 inhibitors potentiate insulin activation of glucose transport and utilization in vitro and in vivo. Diabetes. 52(3):588–595. doi:10.2337/diabetes.52.3.588.

Rodier F, Bahadur RP, Chakrabarti P, Janin J. 2005. Hydration of protein-protein interfaces. Proteins Struct Funct Bioinform. 60:36–45. doi:10.1002/prot.20478.

Salmaso V, Moro S. 2018. Bridging molecular docking to molecular dynamics in exploring ligand-protein recognition process: an overview. Front Pharmacol. 9:923. doi:10.3389/fphar.2018.00923.

Scuto A, Kirschbaum M, Buettner R, Kujawski M, Cermak JM, Atadja P, Jove R. 2013. SIRT1 activation enhances HDAC inhibition-mediated upregulation of GADD45G by repressing the binding of NF-κB/STAT3 complex to its promoter in malignant lymphoid cells. Cell Death Dis. 16;4(5):e635. doi:10.1038/cddis.2013.159.

Seo MH, Park J, Kim E, Hohng S, Kim HS. 2014. Protein conformational dynamics dictate the binding affinity for a ligand. Nat Commun. 24;5:3724. doi:10.1038/ncomms4724.

Siddiqui-Jain A, Drygin D, Streiner N, Chua P, Pierre F, O'Brien SE, Bliesath J, Omori M, Huser N, Ho C, et al. 2010. CX-4945, an orally bioavailable selective inhibitor of protein kinase CK2, inhibits prosurvival and angiogenic signaling and exhibits antitumor efficacy. Cancer Res. 70 (24):10288–10298. doi:10.1158/0008-5472.CAN-10-1893.

Sisay M. 2020. 3CLpro inhibitors as a potential therapeutic option for COVID-19: available evidence and ongoing clinical trials. Pharmacol Res. 156:104779. doi:10.1016/j.phrs.2020.104779.

Solt LA, Kumar N, Nuhant P, Wang Y, Lauer JL, Liu J, Istrate MA, Kamenecka TM, Roush WR, Vidović D, et al. 2011. Suppression of TH17 differentiation and autoimmunity by a synthetic ROR ligand. Nature. 472(7344):491–494. doi:10.1038/nature10075.

Solt LA, Wang Y, Banerjee S, Hughes T, Kojetin DJ, Lundasen T, Shin Y, Liu J, Cameron MD, Noel R, et al. 2012. Regulation of circadian behaviour and metabolism by synthetic REV-ERB agonists. Nature. 485(7396):62–68. doi:10.1038/nature11030.

Sultan A. 2019. Identification and development of clock-modulating small molecules - an emerging approach to fine-tune the disrupted circadian clocks. Biol Rhythm Res. 50(5):769–786. doi:10.1080/09291016.2018.1498197.

Trott O, Olson AJ. 2010. AutoDockVina: improving the speed and accuracy of docking with a new scoring function, efficient optimization, and multithreading. J Comput Chem. 31 (2):455–461. doi:10.1002/jcc.21334.

Ursu A, Illich DJ, Takemoto Y, Porfetye AT, Zhang M, Brockmeyer A, Janning P, Watanabe N, Osada H, Vetter IR, et al. 2016. Epiblastin A induces reprogramming of epiblast stem cells into embryonic stem cells by inhibition of casein kinase 1. Cell Chem Biol. 23(4):494–507. doi:10.1016/j.chembiol.2016.02.015.

Wagner FF, Bishop JA, Gale J, Shi X, Walk M, Ketterman J, Patnaik D, Barker D, Walpita D, Campbell AJ, et al. 2016. Inhibitors of glycogen synthase kinase 3 with exquisite kinome-wide selectivity and their functional effects. ACS Chem Biol. 11:1952e1963. doi:10.1021/acschembio.6b00306.

Walton KM, Fisher K, Rubitski D, Marconi M, Meng QJ, Sládek M, Adams J, Bass M, Chandrasekaran R, Butler T, et al. 2009. Selective inhibition of casein kinase 1 epsilon minimally alters circadian clock period. J Pharmacol Exp Ther. 330(2):430–439. doi:10.1124/jpet.109.151415.

Wang M, Cao R, Zhang L, Yang X, Liu J, Xu M, Shi Z, Hu Z, Zhong W, Xiao G. 2020. Remdesivir and chloroquine effectively inhibit the recently emerged novel coronavirus (2019-nCoV) in vitro. Cell Res. 30(3):269–271. doi:10.1038/s41422-020-0282-0.

Wang Y, Kumar N, Nuhant P, Cameron MD, Istrate MA, Roush WR, Griffin PR, Burris TP. 2010. Identification of SR1078, a synthetic agonist for the orphan nuclear receptors RORα and RORγ. ACS Chem Biol. 5(11):1029–1034. doi:10.1021/cb100223d.

World Health organization. 2020. Clinical management of COVID-19: interim guidance, 27 May 2020. World Health Organization. https://apps.who.int/iris/handle/10665/332196

Wu A, Peng Y, Huang B, Ding X, Wang X, Niu P, Meng J, Zhu Z, Zhang Z, Wang J, et al. 2020a. Genome composition and divergence of the novel coronavirus (2019-nCoV) originating in China. Cell Host Microbe. 27(3):325–328. doi:10.1016/j.chom.2020.02.001.

Wu F, Zhao S, Yu B, Chen YM, Wang W, Song ZG, Hu Y, Tao ZW, Tian JH, Pei YY, et al. 2020b. A new coronavirus associated with human respiratory disease in China. Nature. 579(7798):265–269. doi:10.1038/s41586-020-2008-3.

Wu JT, Leung K, Leung GM. 2020c. Nowcasting and forecasting the potential domestic and international spread of the 2019-nCoV outbreak originating in Wuhan, China: a modelling study. Lancet. 395(10225):689–697. doi:10.1016/S0140-6736(20)30260-9.

Yadav DK, Kumar S, Saloni MS, Yadav L, Teli M, Sharma P, Chaudhary S, Kumar N, Choi EH, Kim HS, et al. 2018. Molecular insights into the interaction of RONS and Thieno [3,2-c]pyran Analogs with SIRT6/COX-2: a molecular dynamics study. Sci Rep. 8(1):4777. doi:10.1038/s41598-018-22972-9.

Yan Y, Shin WI, Pang YX, Meng Y, Lai J, You C, Zhao H, Lester E, Wu T, Pang CH. 2020. The first 75 days of novel coronavirus (SARS-CoV-2) outbreak: recent advances, prevention, and treatment. Int J Environ Res Public Health. 17 (7):2323. doi:10.3390/ijerph17072323.

Yang H, Yang M, Ding Y, Liu Y, Lou Z, Zhou Z, Sun L, Mo L, Ye S, Pang H, et al. 2003. The crystal structures of severe acute respiratory syndrome virus main protease and its complex with an inhibitor. Proc Natl Acad Sci USA. 100(23):13190–13195. doi:10.1073/pnas.1835675100.

Ye T, Wei L, Shi J, Jiang K, Xu H, Hu L, Kong L, Zhang Y, Meng S, Piao H. 2019. Sirtuin1 activator SRT2183 suppresses glioma cell growth involving activation of endoplasmic reticulum stress pathway. BMC Cancer. 19(1):706. doi:10.1186/s12885-019-5852-5.

Zhang KE, Wu E, Patick AK, Kerr B, Zorbas M, Lankford A, Kobayashi T, Maeda Y, Shetty B, Webber S. 2001. Circulating metabolites of the human immunodeficiency virus protease inhibitor nelfinavir in humans: structural identification, levels in plasma, and antiviral activities. Antimicrob Agents Chemother. 45(4):1086–1093. doi:10.1128/AAC.45.4.1086-1093.2001.

Zhang L, Lin D, Sun X, Curth U, Drosten C, Sauerhering L, Becker S, Rox K, Hilgenfeld R. 2020. Crystal structure of SARS-CoV-2 main protease provides a basis for design of improved α-ketoamide inhibitors. Science. 368 (6489):409–412. doi:10.1126/science.abb3405.

Zhang YZ, Holmes EC. 2020. A genomic perspective on the origin and emergence of SARS-CoV-2. Cell. 181 (2):223–227. doi:10.1016/j.cell.2020.03.035.

Zhong H, Wang Y, Zhang ZL, Liu YX, Le KJ, Cui M, Yu YT, Gu ZC, Gao Y, Lin HW. 2020. Efficacy and safety of current therapeutic options for COVID-19 - lessons to be learnt from SARS and MERS epidemic: a systematic review and meta-analysis. Pharmacol Res. 157:104872. doi:10.1016/j.phrs.2020.104872.

Zhou P, Yang XL, Wang XG, Hu B, Zhang L, Zhang W, Si HR, Zhu Y, Li B, Huang CL, et al. 2020. A pneumonia outbreak associated with a new coronavirus of probable bat origin. Nature. 579(7798):270–273. doi:10.1038/s41586-020-2012-7.